

A universal set of gates for defect qubits in diamond and silicon carbide

Dmitry Solenov,¹ Sophia E. Economou,¹ and T. L. Reinecke¹

¹*Naval Research Laboratory, Washington, District of Columbia 20375, USA*

We propose a fast scalable optical design for single and two-qubit gates for defect qubits in diamond (NV centers) and in silicon carbide, which are promising candidates for room temperature quantum computing. Two-qubit gates are mediated by microcavity photons that are coupled to optical transitions in these systems. Single-qubit operations are based on optically-assisted selectivity of microwave control. This approach does not require tunability of electronic transitions of the defects, and the cavity mode frequency remains off-resonance with the optical transitions at all times. The gates are controlled by near-resonant narrow-bandwidth optical pulses. We perform full quantum numerical modeling of the proposed gates and show that high fidelities can be obtained.

Qubits encoded by electron states of defects in diamond and in silicon carbide have become promising candidates for room temperature quantum information processing. Long coherence times of $\sim 50 - 200\mu\text{s}$, initialization, readout and single qubit operations have been demonstrated [1, 2] for qubits in both systems at room temperature. Simple entangling operations have been demonstrated on the system of a negatively charged nitrogen vacancy center (NV) in diamond coupled to a nearest carbon (C) [3, 4] or a nearest nitrogen (N) [5, 6] nuclear spin. However these systems are not scalable. Entangling operations of two distant NV qubits have recently been performed in a challenging, state-of-the-art experiment by joint measurement of the photons emitted by the two NV centers [7]. The challenges associated with using this type of entanglement in a quantum information processor pose stringent requirements on the frequencies of the NV centers. Further, the approach is of probabilistic nature,—only $\sim 3\%$ of the emitted photons come from the zero phonon line of the NV center [7]—resulting in a low rate of successful operations. It has also been proposed that nitrogen defect nuclear spins in diamond might potentially be used to mediate a long-range interaction between distant NV qubits [5]. However, introduction of a large number of defect nuclear spins as well as problems caused by imprecise defect positioning in such systems make them impractical. Thus, experimentally viable deterministic two-qubit gates between distant defect qubits remains an important challenge.

Recent developments in photonic microcavities in both diamond [8, 9] and in silicon carbide [10] have opened opportunities to couple distant defect qubits via cavity photons. Microcavities in these systems have been fabricated in either ring [8] or void-pillar geometries [9] with defect qubits placed near the surface. High quality factors of optical modes and large values of photon coupling to the defect optical transitions have been reported for both diamond and silicon carbide systems [8, 10, 11]. This has made photon-mediated distant qubit-qubit interactions experimentally accessible.

We propose a robust optical design for a universal set of deterministic gates in diamond and in silicon carbide

systems using microcavity photons to mediate interactions. We show that two distant defect qubits can be coupled to cavity photons via a two stage optical activation scheme. This approach does not require fine tuning between cavity mode frequency and optical transition frequencies of the defects, which remain off-resonance with the cavity mode. This leads to effective isolation of the single-defect excitations in each qubit, which are used to perform fast optical single-qubit rotations and readout. The excited states involving two defects decouple from the cavity at substantially larger detunings. These states can be used to mediate a qubit-qubit interaction and perform a two-qubit control-Z (CZ) gate. By combining these optical operations with simple global microwave rotations we construct a universal set of gates for scalable architectures aimed at room temperature quantum computing. We perform full quantum mechanical simulations and find that high values of fidelity can be achieved for experimentally reasonable parameters [11–13].

For definiteness we will focus mainly on the case of NV in diamond. The properties of defect centers in silicon carbide are similar [14, 16–18]. The NV defect has eight states of interest [14, 15] (see Fig. 1), six of which, denoted from symmetry considerations as $^3A_{2m}$ and 3E_m ($m = 0, \pm 1$), participate in optical transitions. The other two 1A_1 and 1E typically involve non-radiative recombination with emission of phonons [14]. An external magnetic field, B , splits the states with different ($m = \pm 1$) spin. The qubit is typically encoded by states $|0\rangle = |^3A_{2m=0}\rangle$ and $|1\rangle = |^3A_{2m=-1}\rangle$ and is manipulated with microwave pulses [1, 2, 5, 6]. The excited states 3E_m are typically used to initialize the qubit to the ground state $|0\rangle$ and to read its state. These procedures rely on the differences in recombination times for states with different spin m and are performed similarly for diamond and silicon carbide defect qubits [1, 2, 14, 19].

The optical transitions $^3A_{2m} \leftrightarrow ^3E_m$ are spin conserving. Their frequencies depend on the local environment and therefore are different for different defects [18, 20, 21]. Often, in order to couple two qubits via a cavity mode, transitions in each qubit have to be

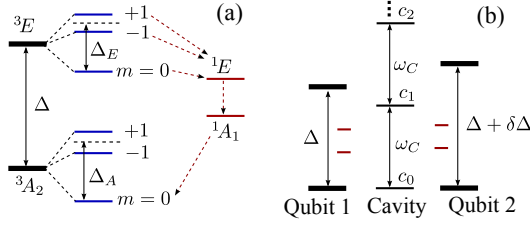


Figure 1: Nitrogen-vacancy center (NV) in diamond as a qubit. (a) The relevant states of the NV in diamond [14]. The qubit is encoded by states ${}^3A_{2m=0}$ and ${}^3A_{2m=-1}$. Non-radiative decay of excited states takes place via 1E and 1A_1 (red) [14]. (b) Two such qubit systems with unequal energies of excited states 3E interacting via a microcavity photon of frequency ω_C are used to perform control-Z (CZ) gate.

tuned dynamically into resonance with the cavity mode to enable the interaction for a period of time thus performing the gate [22, 23]. Instead, we use the natural spectral differences between the defects to our advantage to perform single- and two-qubit phase-control gates via optical pulses. The qubits remain off-resonance with the cavity. A single qubit phase gate is defined as $Z(\theta) = \exp(i\theta\sigma_z/2)$. It acts to add a phase θ to one of the qubit states $A|0\rangle + B|1\rangle \rightarrow A|0\rangle + B|1\rangle e^{i\theta}$. The simplest two-qubit phase-control gate, the control-Z (CZ) gate, is defined by $A|00\rangle + B|01\rangle + C|10\rangle + D|11\rangle \rightarrow A|00\rangle + B|01\rangle + C|10\rangle - D|11\rangle$.

Defects in diamond or silicon carbide in a microcavity are about a μm away from each other or closer. Such proximity makes it difficult to perform individual single-qubit operations with microwave pulses. However, we show that optically-assisted selectivity of microwave control can be achieved even when the microwave field is applied to the entire system, performing simultaneous operations on all qubits. The selectivity can be achieved by inserting a single-qubit optical $Z_i(\theta)$ gate acting on i th qubit between the two conjugate microwave operations \mathbf{X} and $\bar{\mathbf{X}} = \mathbf{X}^{-1}$ acting on all qubits simultaneously. The particular choice of \mathbf{X} is not important, and we will use $\mathbf{X} = X(\pi/2) \otimes X(\pi/2)$ and $\bar{\mathbf{X}} = X(-\pi/2) \otimes X(-\pi/2)$ with $X(\theta) = \exp(i\theta\sigma_x/2)$ to illustrate the procedure. When both conjugate operations are performed on a two-qubit state, it remains unaffected, i.e., $\mathbf{X}\bar{\mathbf{X}}|\Psi\rangle = |\Psi\rangle$. However, if an optical $Z_i(\theta)$ is performed on one (i -th) qubit between \mathbf{X} and $\bar{\mathbf{X}}$, an arbitrary single-qubit rotation is carried out. For example, $Y_i(\theta) = \mathbf{X}Z_i(\theta)\bar{\mathbf{X}}$ and $X_i(\theta) = Y_i(-\pi/2)Z_i(\theta)Y_i(\pi/2)$ together with $Z_i(\theta)$ provide an arbitrary single qubit gate for the i -th qubit. Single qubit operations together with the CNOT $= Y_2(-\pi/2)\text{CZ}Y_2(\pi/2)$ entangling gate, where $Y(\theta) = \exp(i\theta\sigma_y/2)$, form a standard universal set of gates [22].

To see how $Z_i(\theta)$ and CZ can be constructed in our physical system, we consider the spectrum of the two NV defects in a microcavity (see Fig. 2). In the rotating wave

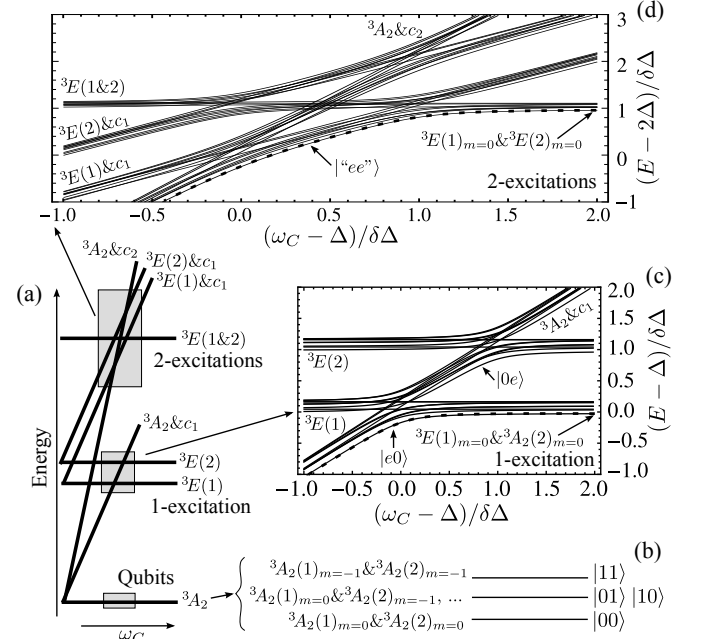


Figure 2: The spectrum of two NV centers interacting with a cavity mode. (a) Schematic depiction of the spectrum for varying values of ω_C . The spectrum can be classified according to the total number of optical excitations. The zero-excitation part, shown in panel (b), is used to encode qubits. Panel (c) shows the part of the spectrum with one excitation, and panel (d) the part with two excitations. Standard symmetry notations are used to label the energy states. In ${}^3A_2 \& c_1$ each defect is in 3A_2 state and there is one photon in a cavity (c_1). Notation ${}^3E(1)$ is used to show that the first defect is in state 3E (while the second is in state 3A_2 with no optical excitation, and the cavity has no photons). The black dashed curves in (c) and (d) mark the excited states used to perform CZ gate.

approximation, the spectrum is given by the Hamiltonian

$$H_0 = \sum_{\mathfrak{A}, i, m=0, \pm 1} \varepsilon_{\mathfrak{A}}^{\mathfrak{A}}(i) |\mathfrak{A}(i)_m\rangle \langle \mathfrak{A}(i)_m| + \sum_{\mathfrak{B}, i} \varepsilon_{\mathfrak{B}}(i) |\mathfrak{B}(i)\rangle \langle \mathfrak{B}(i)| + \omega_C a^\dagger a + \gamma \sum_{i=1,2; m=0, \pm 1} (|{}^3A_2(i)_m\rangle \langle {}^3E(i)_m| a^\dagger + h.c.), \quad (1)$$

where $\mathfrak{A} \in \{{}^3A_2, {}^3E\}$, $\mathfrak{B} \in \{{}^1A_1, {}^1E\}$, $\varepsilon_{\mathfrak{A}}^{{}^3A_2}(i) = |m|\Delta_A + mgB$ and $\varepsilon_{\mathfrak{A}}^{{}^3E}(i) = \Delta + \delta_{i,2}\delta\Delta + |m|\Delta_E + mgB$. The values for the energies $\varepsilon_{\mathfrak{B}}(i)$ of the states 1A_1 and 1E are not important for the following discussion. The Hamiltonian (1) conserves the total number of excitations $\mathcal{N} = \sum_{i,m} |{}^3E(i)_m\rangle \langle {}^3E(i)_m| + a^\dagger a$ and can be diagonalized in each excitation subspace independently. The general structure of the states as functions of the cavity mode frequency ω_C is shown in Fig. 2(a). The qubit subspace states $|00\rangle$, $|01\rangle$, $|10\rangle$ and $|11\rangle$ [Fig. 2(b)] are unaffected by the cavity mode. At higher energies electron and cavity states mix. The resulting structure shown in Fig. 2(c-d) is formed by a collection of simple avoided-crossings that involve only a few states due to optical

selection rules of the Hamiltonian (1).

In the one-excitation part of the spectrum [Fig. 2(c)] the states are coupled in groups of three involving two anti-crossings: the excited states of each of the two NV's in the same spin configuration interact with the cavity photon state. When the energies of the excited states are sufficiently far from each other, the two anti-crossings effectively separate resulting in local (i.e., isolated from one another) electron-photon states, e.g., $|e\rangle$ in Fig. 2(c). In this case the interaction between the two defects decreases rapidly as $\sim \gamma\Delta_A/\delta\Delta^2$ and for typical values of $\gamma/\delta\Delta \sim \Delta_A/\delta\Delta \sim 0.01$ can be neglected. The decrease of the interaction is seen by noting that there are two off-resonant transitions involving a cavity photon, each adding a factor of $1/\delta\Delta$. As a result, the single-excitation sector is ideal to perform local (single-qubit) optical $Z(\theta)$ operations, as in Ref. [24] for $Z_i(\theta)$ gate. The transition between states $|00\rangle$ and $|e0\rangle$ [Fig. 2(c)] is addressed with a single off-resonant 2π (or cyclic) pulse. For the above values of $\gamma/\delta\Delta$ the energy difference between states $|01\rangle$ and $|e1\rangle$ is nearly identical to that in between $|00\rangle$ and $|e0\rangle$, and thus only the first qubit is affected by the control pulse. An optical pulse field can be added to the Hamiltonian as

$$\Omega_p(t-t_p)\cos\omega_pt\sum_{m=0,\pm1}(|^3A_2(i)_m\rangle\langle^3E(i)_m|+h.c.), \quad (2)$$

where Ω_p and ω_p are the Rabi and carrier frequencies of the laser pulse. For certain shapes of $\Omega_p(t)$ [25] a cyclic pulse is produced in which the entire population of the state $|0\rangle$ of the first qubit is transferred to state $|e\rangle$ and back. The phase accumulated during the pulse, $|0\rangle \rightarrow |e\rangle \rightarrow |0\rangle e^{i\theta}$, depends on the detuning of ω_p from the frequency of the transition and on the pulse shape Ω_p . A $Z_2(\theta)$ operation is similar and is based on state $|0e\rangle$; see Fig. 2(c).

We now consider the cavity-induced effective interaction between the defect qubits in the two-excitation subspace [see Fig. 2(d)]. The effective interaction in the two-excitation subspace is greater than that in the one-excitation subspace. The energy of the state $|ee\rangle$, which involves excitations in both defects and a photon [see Fig. 2(d)], differs from the combined energies of states $|0e\rangle$ and $|e0\rangle$, which involve excitation of only one of the defects. This is the basis for “on-demand” qubit-qubit coupling. The state $|ee\rangle$, however, is not directly accessible with an optical field. It can be reached only if the system is first transferred into the one-excitation subspace, e.g. $|e0\rangle$. This can be done with a $\int dt\Omega(t) = \pi$ resonant pulse tuned to the corresponding transition. After that, a $\int dt\Omega(t) = 2\pi$ resonant cyclic pulse tuned to the transition between $|e0\rangle$ and $|ee\rangle$ can be used to perform a $Z_2(2\pi)$ operation if and only if the first qubit was in state $|0\rangle$. Such conditionality is rooted in the difference between the energy of $|ee\rangle$ and the sum of energies of $|0e\rangle$ and $|e0\rangle$ for non-zero γ . If $\gamma = 0$ this energy differ-

ence is zero and the state $|ee\rangle$ is the product $|e\rangle|e\rangle$ and the second pulse produces a (unconditional) single-qubit $Z_2(2\pi)$ rotation. After the conditional $Z_2(2\pi)$ rotation, the system must be restored to the qubit subspace with the pulse identical to the first one. The pulse sequence to perform CZ gate is shown in Fig. 3(a).

The coherence of the proposed single- and two-qubit gates is determined by the fidelity of their components—microwave rotations and optical pulse-controlled phase gates. The fidelity of the microwave rotations is limited primarily by decoherence of the qubits. In diamond and silicon carbide systems the time scale of the qubit decoherence is large $\sim \mu s$ [1, 2]. In the optical gates, decoherence can take place at a much shorter time scale. In this case there are two sources of possible fidelity loss: (i) destructive interference due to transitions that were not accounted for, and (ii) real losses due to radiative and non-radiative recombination of the excited electron states as well as loss of photons from the cavity. Decoherence during a single qubit $Z_i(\theta)$ operation is similar to that due to the first pulse in the CZ gate. Therefore a lower bound to fidelity of the proposed gates can be obtained by calculating the fidelity of a single CZ gate. We include all eight states shown in Fig. 1(a) for each qubit and ten states to represent the cavity mode in our numerical modeling. The fidelity of the CZ gate is evaluated from the reduced density matrix of the two-qubit system before, $\rho(0)$, and after, $\rho = \rho(t_g)$, the gate. The evolution is computed using the Bloch-Redfield Master equation $i\dot{\rho} = [H + V(t), \rho] + \sum_s i\Gamma_s L_s \{\rho\}$ where $L_s = [P_s \rho P_s^\dagger - (P_s^\dagger P_s \rho + \rho P_s^\dagger P_s)/2]$ [22, 26]. We take the state $\rho(0)$ to be a pure state $|\psi_0\rangle\langle\psi_0|$. The fidelity of the gate operation is given by $F(\psi_0, \rho\{\psi_0\}) = (\langle\psi_0|U_{CZ}^\dagger \rho U_{CZ}|\psi_0\rangle)^{1/2}$. In quantum computation the state ψ_0 can vary depending on the input data and the algorithm involved. To estimate the decoherence introduced by the gate in an arbitrary circuit, we compute the fidelity averaged over the initial state [29, 30]

$$F^2 = \sum_{ijnm=\{1,4\}} \frac{\delta_{in}\delta_{jm} + \delta_{ij}\delta_{nm}}{20} \langle n|U_{CZ}^\dagger \rho\{|i\rangle\langle j|\}U_{CZ}|m\rangle \quad (3)$$

The resulting fidelity is shown in Fig. 3(b-c). In Fig. 3(b) we plot the fidelity optimized over the values of pulse bandwidth σ as a function of pulse separation time δt for cavity quality factors in the range $\Delta/\gamma Q = \{0.003, 0.1\}$ μeV . The values for recombination rates in NV defects ($\sim 10 ns$) were taken from [14]. We used $\gamma = 15 \mu eV$, $\delta\Delta = 100 \mu eV$, and $gB = 0.1 \mu eV$ in Fig. 3. We find that the maximum fidelity is reached when pulses overlap thus reducing decoherence. The fidelity as a function of σ and Q is shown in Fig. 3(c) for $\sigma\delta t = 3$. The fidelity peaks at $\sigma/\gamma \sim 0.2$ and is smaller for higher and lower values of σ due to unintended dynamics and real losses, respectively. The fidelity of the CZ gate applied to silicon-carbide defect qubits is qualitatively similar but

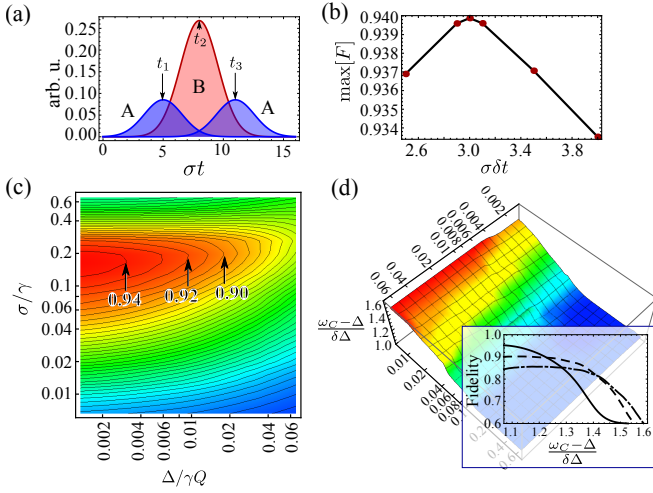


Figure 3: Fidelity of the CZ gate. (a) Pulse sequence used. (b) Variation of fidelity as function of spacing $\delta t = t_2 - t_1 = t_3 - t_2$ between the pulses. The maximum value of fidelity over the range of σ 's and Q 's of panel (c) is shown. (c) Fidelity as a function pulse bandwidth, σ , and cavity quality factor, Q . Each point corresponds to the optimal placement of the cavity mode frequency ω_C relative to the energies of the excited states, as shown in panel (d). Inset in panel (d) shows fidelity as a function of ω_C at $\Delta/\gamma Q = 1.3 \times 10^{-3}$ and with $\sigma/\gamma = 0.17, 0.05$, and 0.03 , given by solid, dashed, and dashed-dotted curves respectively.

involves recombination rates specific to that system. In both figures we chose optimal values of the cavity frequency ω_C with respect to the excitation energies of the defects. The optimal ω_C for each point of Fig. 3(c) is shown in Fig. 3(d). Typically the gate fidelity as a function of ω_C has a wide plateau of high values [see the inset in Fig. 3(d)], and then it decreases when ω_C is far above or below Δ . As a result, precise positioning of the defect and cavity energy levels with respect to each other is not necessary. A similar procedure for a CZ gate can be formulated using the second qubit as a conditional qubit, in which case high fidelities will be reached at $\omega_C - \Delta < 0$ in a symmetric fashion. In both cases the fidelity of the gate becomes small when ω_C is far off resonance with Δ and $\gamma/\delta\Delta$ becomes vanishingly small. The maximum fidelity of the gates is limited primarily by the cavity Q . Thus, in order to operate, the gates require the strong coupling regime, which is given by $\Delta/\gamma Q \ll 1$.

We have demonstrated that the fidelity of the proposed universal set of gates can reach high values. The single and two-qubit operations are performed using different classes of states in the excitation spectrum of the system, and are not very sensitive to the positioning of the cavity mode frequency with respect to the defect energies. This can be used to couple multiple spectrally distinct defects pairwise using a single cavity mode without loss of fidelity due to their cross-talk. Thus, this cavity-based design has an advantage of scalability in these systems.

Additional scalability can be obtained by coupling several cavity systems via wave guides.

This work was supported by the ONR and by NSA/LPS. Computer resources were provided by the DoD HPCMP.

- [1] T. A. Kennedy, J. S. Colton, J. E. Butler, R. C. Linares, and P. J. Doering, *Appl. Phys. Lett.* **83**, 4190 (2003).
- [2] W. F. Koehl, B. B. Buckley, F. J. Heremans, G. Calusine, and D. D. Awschalom, *Nature* **479**, 84 (2011).
- [3] F. Jelezko, T. Gaebel, I. Popa, M. Domhan, A. Gruber, and J. Wrachtrup, *Phys. Rev. Lett.* **93**, 130501 (2004).
- [4] M. V. Gurudev Dutt, L. Childress, L. Jiang, E. Togan, J. Maze, F. Jelezko, A. S. Zibrov, P. R. Hemmer, M. D. Lukin, *Science* **316**, 1312 (2007).
- [5] R. Hanson, F. M. Mendoza, R. J. Epstein, and D. D. Awschalom *Phys. Rev. Lett.* **97**, 087601 (2006).
- [6] T. Gaebel, M. Domhan, I. Popa, C. Wittmann, P. Neumann, F. Jelezko, J. R. Rabeau, N. Stavrias, A. D. Greetree, S. Prawer, J. Meijer, J. Twamley, P. R. Hemmer, and J. Wrachtrup, *Nature Physics* **2**, 408 (2006).
- [7] H. Bernien, B. Hensen, W. Pfaff, G. Koolstra, M. S. Blok, L. Robledo, T. H. Taminiau, M. Markham, D. J. Twitchen, L. Childress, R. Hanson, *arXiv:1212.6136* at www.arXiv.org.
- [8] A. Faraon, P. E. Barclay, C. Santori, Kai-Mei C. Fu, and R. G. Beausoleil, *Nature Photonics* **5**, 301 (2011).
- [9] J. Riedrich-Moller, L. Kipfstuhl, C. Hepp, E. Neu, C. Pauly, A. Baur, M. Wandt, S. Wolff, M. Fischer, S. Gsell, F. Mucklich, M. Schreck, and C. Becher, *Nature Nanotech.* **7**, 69 (2012).
- [10] S. Yamada, B.-S. Song, T. Asano, and S. Noda, *Appl. Phys. Lett.* **99**, 201102 (2011).
- [11] A. Faraon, C. Santori, Z. Huang, V. M. Acosta, and R. G. Beausoleil *Phys. Rev. Lett.* **109**, 033604 (2012).
- [12] M. D. Lukin, private communication (2012)
- [13] A. Faraon, C. Santori, Z. Huang, K.-M. C. Fu, V. M. Acosta, D. Fattal, and R. G. Beausoleil, *New J. Phys.* **15**, 025010 (2013).
- [14] V. M. Acosta, A. Jarmola, E. Bauch, and D. Budker, *Phys. Rev. B* **82**, 201202 (2010).
- [15] J. R. Maze, A. Gali, E. Togan, Y. Chu, A. Trifonov, E. Kaxiras, and M. D. Lukin, *New J. Phys.* **13**, 025025 (2011).
- [16] P. G. Baranova, I. V. Ilina, E. N. Mokhova, M. V. Muza-farova, S. B. Orlinskiib, and J. Schmidt, *JETP Letters* **82**, 441 (2005).
- [17] N. T. Son, P. Carlsson, J. ul Hassan, E. Janzn, T. Umeda, J. Isoya, A. Gali, M. Bockstedte, N. Morishita, T. Ohshima, and H. Itoh, *Phys. Rev. Lett.* **96**, 055501 (2006); A. Gali, A. Gallstrom, N.T. Son, and E. Janzen, *Materials Science Forum* **645-648**, 395 (2010); A. Gali, *Journal of Materials Research* **27**, 897 (2012).
- [18] D. Riedel, F. Fuchs, H. Kraus, S. Vath, A. Sperlich, V. Dyakonov, A. A. Soltamova, P. G. Baranov, V. A. Ilyin, and G. V. Astakhov, *Phys. Rev. Lett.* **109**, 226402 (2012).
- [19] R. Hanson, F. M. Mendoza, R. J. Epstein, and D. D. Awschalom, *Phys. Rev. Lett.* **97**, 087601 (2006).
- [20] A. Batalov, V. Jacques, F. Kaiser, P. Siyushev, P. Neumann, L. J. Rogers, R. L. McMurtrie, N. B. Manson, F.

- Jelezko, and J. Wrachtrup, Phys. Rev. Lett. **102**, 195506 (2009).
- [21] L. C. Bassett, F. J. Heremans, C. G. Yale, B. B. Buckley, and D. D. Awschalom, Phys. Rev. Lett. **107**, 266403 (2011).
 - [22] M. A. Nielsen and I. L. Chuang, Quantum Computation and Quantum Information (Cambridge Univ. Press).
 - [23] A. M. Zagoskin, J. R. Johansson, S. Ashhab, and Franco Nori, Phys. Rev. B **76** 014122 (2007)
 - [24] S. E. Economou, L. J. Sham, Y. Wu, and D. G. Steel, Phys. Rev. B **74**, 205415 (2006).
 - [25] N. Rosen and C. Zener, Phys. Rev. **40**, 502 (1932).
 - [26] This approach is appropriate [27] for evaluation of decoherence due to decay of optically excited states. Decoherence during microwave pulses operating in the qubit subspace is best estimated by “short-time” expansion techniques [28].
 - [27] D. Solenov, D. Tolkunov, and V. Privman, Phys. Rev. B **75**, 035134 (2007).
 - [28] D. Solenov and V. Privman, International Journal of Modern Physics B **20**, 1476 (2006).
 - [29] L. H. Pedersen, N. M. Møller, K. Mølmer, Phys. Lett. A **367**, 47 (2007).
 - [30] Note that the generalization of the expression for the average fidelity found in Ref. [29] is possible because the reduced density matrix after the gate operation is a linear function of the initial reduced density matrix [31].
 - [31] D. Solenov, L. Fedichkin, Phys. Rev. A **73**, 012308 (2006).